

Dense monoenergetic proton beams from chirped laser-plasma interaction

Benjamin J. Galow,¹ Yousef I. Salamin,^{1,2} Tatyana V. Liseykina,³ Zoltán Harman,^{1,4} and Christoph H. Keitel¹

¹*Max-Planck-Institut für Kernphysik, Saupfercheckweg 1, 69029 Heidelberg, Germany*

²*Department of Physics, American University of Sharjah, POB 26666, Sharjah, United Arab Emirates*

³*Institut für Physik, Universität Rostock, 18051 Rostock, Germany*

⁴*ExtreMe Matter Institute EMMI, Planckstrasse 1, 64291 Darmstadt, Germany*

Interaction of a frequency-chirped laser pulse with single protons and a hydrogen gas target is studied analytically and by means of particle-in-cell simulations, respectively. Feasibility of generating ultra-intense (10^7 particles per bunch) and phase-space collimated beams of protons (energy spread of about 1%) is demonstrated. Phase synchronization of the protons and the laser field, guaranteed by the appropriate chirping of the laser pulse, allows the particles to gain sufficient kinetic energy (around 250 MeV) required for such applications as hadron cancer therapy, from state-of-the-art laser systems of intensities of the order of 10^{21} W/cm².

PACS numbers: 52.38.Kd, 37.10.Vz, 42.65.-k, 52.75.Di, 52.59.Bi, 52.59.Fn, 41.75.Jv, 87.56.bd

Interaction of high-intensity lasers with solid targets has attracted much interest over the past decade, due to its potential utilization in laser acceleration of particles [1–13]. This has given much needed impetus to efforts directed at replacing conventional accelerators in the near future by compact and relatively low-cost devices based on an all-optical acceleration mechanism [14]. In particular, hadron cancer therapy [15, 16] may benefit from this trend.

Several regimes are now in existence for laser-plasma acceleration [17]. For laser intensities of $10^{18} - 10^{21}$ W/cm² and solid targets with a thickness ranging from a few to tens of micrometers, target normal sheath acceleration (TNSA) is the prevailing mechanism. In TNSA, a strong quasi-static electric field is induced at the rear surface of a thin foil, as a result of emission and acceleration of the electrons caused by an intense linearly polarized laser field. Ion acceleration, by the sheath electric field, has been extensively studied [1–10]. The regime of radiation-pressure-dominant acceleration (RPA), has become recently accessible by decreasing the target thickness. Circularly polarized lasers at normal incidence have been employed, which suppress electron heating and let all particle species co-propagate as a quasi-neutral plasma bunch in front of the light wave (“light sail”-mechanism) [18]. Despite recent experimental [19] and theoretical [20] progress, clinically useful ion beams [21] have not yet been produced within a scheme which operates at currently available laser parameters.

In this Letter, we demonstrate the theoretical feasibility of creating proton beams, of unprecedented energy and quality, from illuminating a hydrogen gas target with an appropriately chirped laser pulse of intensity accessible by state-of-the-art laser systems [22]. The basic idea of our model stems from the realization that an incoming highly relativistic laser pulse quickly ionizes hydrogen in the cell and accelerates the electrons away from the much heavier protons, as the pulse intensity rises. At high enough laser intensities the protons get accelerated

directly by the laser field. Chirping of the laser pulse ensures optimal phase synchronization among the protons and the laser field and leads to efficient proton energy gain from such a field.

We derive an expression for the energy transfer during interaction of a particle with chirped unfocused as well as pulsed electromagnetic fields. Results obtained analytically for the particle’s energy gain will be supported by further simulations which describe the focused fields more accurately than the simple plane-wave model. Our two-dimensional (2D) particle-in-cell (PIC) simulations reveal that proton beams of energy around 250 MeV, energy spread of about 1%, and density of 10^7 particles per bunch, can be produced. Beams of such quality may potentially be suitable for use in hadron cancer therapy assuming the laser-plasma interaction can take place close to the patient [23]. Following acceleration, the beams have to be collimated and guided [24] to compensate larger variations in the laser pulse and its chirp which is still challenging to control at high intensities. Future laser systems at the ELI or HiPER facilities [25, 26] may be utilized to produce monoenergetic multi-GeV proton beams.

A point particle of mass M and charge Q acquires relativistic energy and momentum, respectively, of $\mathcal{E} = \gamma Mc^2$ and $\mathbf{p} = \gamma Mc\boldsymbol{\beta}$, where $\boldsymbol{\beta}$ is the velocity of the particle scaled by c , the speed of light in vacuum, and $\gamma = (1 - \beta^2)^{-1/2}$, when interacting with the fields \mathbf{E} and \mathbf{B} of an intense laser pulse. It suffices in many applications to represent the fields of the beam by plane waves. A plane wave propagating along the z -axis and polarized along the x -axis, may be represented by $\mathbf{E} = \hat{\mathbf{x}}E_0f$ and $\mathbf{B} = \hat{\mathbf{y}}E_0f/c$. The dependence in f on the space-time coordinates is through the combination $\omega t - kz$, with ω the frequency and $k = \omega/c$ the wave number. This leads to a break-up of the energy-momentum transfer equations (SI units) into four component equations, namely

$$\frac{d}{dt}(\gamma\beta_x) = a\omega_0(1 - \beta_z)f, \quad \frac{d}{dt}(\gamma\beta_y) = 0, \quad (1)$$

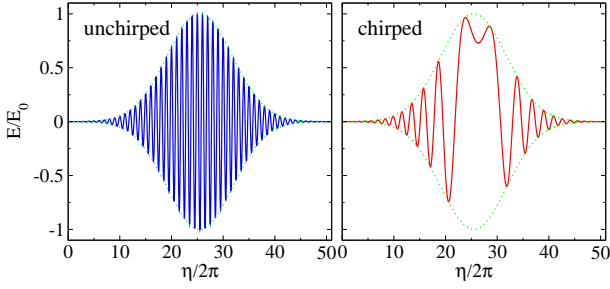


FIG. 1: (color online). The normalized electric field at focus of a plane-wave pulse employing Eq. (5). The parameters used are: $\lambda = 1 \mu\text{m}$, and $\tau = 50 \text{ fs}$, $\phi_0 = 0$ and $\bar{\eta} = 4s$.

$$\frac{d}{dt}(\gamma\beta_z) = a\omega_0\beta_x f, \quad \frac{d\gamma}{dt} = a\omega_0\beta_x f, \quad (2)$$

where $a = QE_0/(Mc\omega_0)$ is a normalized laser field strength and ω_0 will be defined below. From the second of Eqs. (1) we immediately identify a first constant of the motion, namely $\gamma\beta_y = c_1$. Furthermore, the constant $\gamma(1 - \beta_z) = \gamma_0(1 - \beta_{z0}) = c_2$ may be arrived at by subtracting the second of Eqs. (2) from the first, and integrating. Substituting the constants c_1 and c_2 via β_y and β_z into $\gamma^{-2} = 1 - (\beta_x^2 + \beta_y^2 + \beta_z^2)$, the following key expression for the energy of the particle, scaled by its rest energy, may be arrived at

$$\gamma = \frac{1 + (\gamma\beta_x)^2 + c_1^2 + c_2^2}{2c_2}. \quad (3)$$

The combination $\eta = \omega_0(t - z/c)$ will be used often below. Note that with the help of $d\eta/dt = \omega_0(1 - \beta_z)$, the first of Eqs. (1) may be formally integrated to give

$$\gamma\beta_x = \gamma_0\beta_{x0} + a \int_{\eta_0}^{\eta} f(\eta') d\eta', \quad (4)$$

where $\beta_{x0} = \beta_x(\eta_0)$ and $\gamma_0 = (1 - \beta_0^2)^{-\frac{1}{2}}$.

Frequency chirping amounts to letting ω vary with time in some fashion. Experimentally, laser pulses with a near-uniform spectral intensity over two octaves are feasible [27]. The phase-coherent synthesis of separate femtosecond lasers [28] and the recent synthesis of multiple optical harmonics [29] put forward lasers with an even wider frequency range. We will work with the linear chirp $\omega = \omega_0 + b_0(t - z/c)$ [30–32], with ω_0 denoting the frequency at $t = 0$ and $z = 0$, and b_0 having a unit of s^{-2} . The chirped frequency thus becomes $\omega = \omega_0(1 + b\eta)$, where $b = b_0/\omega_0^2$ is a dimensionless chirp parameter. Also, dependence of the fields on the space-time coordinates may be rewritten as $\omega t - kz \rightarrow \eta + b\eta^2$, and the chirped field function $f(\omega t - kz) \rightarrow f(\eta + b\eta^2)$. We will initially work with

$$f = \cos(\phi_0 + \eta + b\eta^2)g(\eta); \quad g(\eta) = \exp\left(-\frac{(\eta - \bar{\eta})^2}{2s^2}\right), \quad (5)$$

where ϕ_0 is a constant initial phase, $g(\eta)$ a pulse-shape function, and s is related to the pulse duration τ (full-width at half-maximum) via $s = \omega_0\tau/(2\sqrt{2}\ln 2)$. In our calculations, we choose a shift in η in the envelope function $g(\eta)$ denoted by $\bar{\eta} = 4s$. Eq. (5) approximates an actual laser pulse in which the non-vanishing pulse integral may be compensated by a quasi-static tail.

To illustrate the mechanism of acceleration, we show in Fig. 1 the normalized electric field E/E_0 as a function of η . Interaction of a particle with the unchirped pulse will result in no energy gain, due to the plane-wave symmetry: gain from a positive part of the field gets canceled by loss to an equally strong negative part. However, the chirping breaks this symmetry. Thus, interaction with the low-frequency and strong positive part of the chirped pulse, which extends over roughly one half of the pulse duration, results in net energy gain.

For a particle initially ($\eta = \eta_0$) at rest, $c_1 = 0$ and $c_2 = \gamma_0 = 1$. Thus, Eqs. (3) and (4) give the following expression for evolution in η of the particle kinetic energy

$$K(\eta) = (\gamma - 1)Mc^2 = \frac{Mc^2}{2}(\gamma\beta_x)^2. \quad (6)$$

Using the initial conditions and Eqs. (4) and (5), Eq. (6) can be analytically integrated in terms of a complex error function. Thus, Eq. (6) gives the kinetic energy of the particle explicitly, and helps us determine the value of the chirp parameter b that maximizes it. Note from Eqs. (4) and (6) that the proton energy scales linearly with the laser intensity.

In order to test the applicability of the analytic plane-wave model, we compare results based on it with those stemming from the use of focused laser fields. For the focused fields, the Lax series expressions will be adopted, according to which all components E_x, E_y, E_z, B_y , and B_z [33] are given in powers of the diffraction angle $\varepsilon = \lambda/\pi w_0$, where w_0 is the waist radius of the beam at focus. Simulations are performed to solve the equations of motion numerically for a single proton submitted to the laser fields from an initial position of rest at the origin of coordinates ($\eta_0 = 0$). In the simulations, $w_0 = 5\lambda$ gives $\varepsilon = 1/5\pi \ll 1$. Hence, terms in the Lax series up to $\mathcal{O}(\varepsilon^2)$ only need to be retained. The simulations demonstrate clearly that the two models predict exit kinetic energies that agree to within 2–3% for the parameters used in Fig. 2. The linear scaling of the exit kinetic energy with the laser intensity given by the plane-wave model only holds true for intensities up to about $5 \times 10^{21} \text{ W/cm}^2$. For highly relativistic particles the exit kinetic energy scales as the square root of the laser intensity, which is the case in conventional TNSA [4], too.

In Fig. 2 (a) and (b) the exit kinetic energy K of a single proton is displayed as a function of b in the limit of large η and for optimal b as a function of $\eta/2\pi$, respectively. The energy gain is found to peak globally at the chirp parameter values of $b \sim -0.003033$ and -0.002979

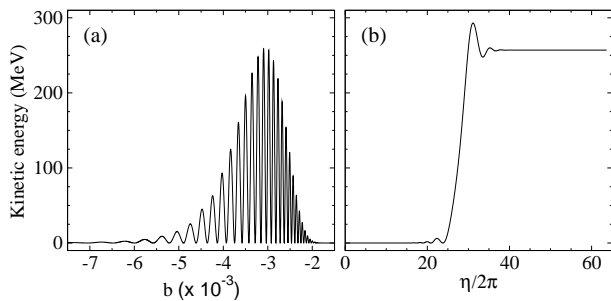


FIG. 2: (a) Exit kinetic energy gained by one proton as a function of the dimensionless chirp parameter b in the limit of large η . (b) Evolution of the proton kinetic energy with $\eta/2\pi$ for optimal $b = -0.002979$. Peak power of the focused laser system is 1 PW, which corresponds to a peak intensity of 2.55×10^{21} W/cm² for $w_0 = 5\lambda$, $\tau = 50$ fs and $\lambda = 1 \mu\text{m}$. Other parameters used are: $\phi_0 = 0$, and $\bar{\eta} = 4s$.

for the plane-wave and focused pulses, respectively, and for the specific laser system parameter set used. Other optimal chirp parameter values, which can be determined in like fashion, lead to local, less pronounced kinetic energy maxima. The fact that the optimal values of b are so close (and so are the corresponding exit kinetic energies) demonstrates that the analytic solution can be quite reliable and that the plane-wave representation closely describes the physics involved, at least for the parameter set used in which $w_0 \gg \lambda$. On the other hand, it is obvious that dependence upon b of the exit particle kinetic energy is sensitive, especially in the regime where high energy is sought. In fact, the plane-wave calculation yields the uncertainty $\delta K \approx 1/2(\partial^2 K/\partial b^2)|_b(\delta b)^2$, which results from an uncertainty $\delta b \sim 10^{-6}$ in determining b . The plane-wave calculation yields $\delta K \sim 0.195$ MeV, or about 0.074%. When one takes $\delta b \sim 10^{-5}$ instead, the uncertainties increase by two orders of magnitude ($\delta K \sim 19.5$ MeV and 7.4%).

Having studied the single-particle aspects, we now present typical 2D3V-PIC (two spatial dimensions and three momentum space degrees of freedom) simulation results of the interaction of the chirped laser pulse with a pre-ionized hydrogen target. The target might be either an expanding hydrogen cluster available at sizes ranging from 1 nm to $1 \mu\text{m}$ [34] or part of a hydrogen gas jet. We are using the following simulation environment: The spatial resolution of our simulation box is given by $\Delta z = \Delta x = \lambda/100$, where the laser wavelength is still assumed to be $\lambda = 1 \mu\text{m}$. The particle number per cell is 100, for both protons and electrons. The x -polarized laser enters the simulation box from the left and propagates in the z -direction. For the fields we choose a simple modification of the plane wave fields given by $\mathbf{E} = \hat{x}E_0 f e^{-x^2/(2w_0^2)}$ and $\mathbf{B} = \hat{y}(E_0/c) f e^{-x^2/(2w_0^2)}$, with f from Eq. (5) and the factor $e^{-x^2/(2w_0^2)}$ mimicking spatial focusing in the polarization direction. The target dimensions are assumed to have a length of 0.2λ in the

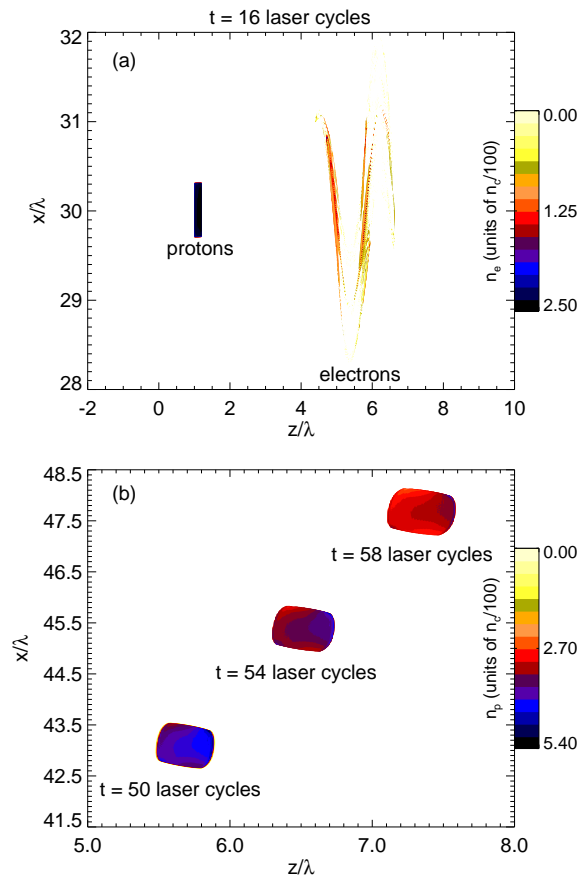


FIG. 3: (color online). Snap-shots (a) of the electron and proton density distribution during laser-plasma interaction and (b) of the proton density distribution after laser-plasma interaction for various times. The laser peak intensity is 2.55×10^{21} W/cm² with $w_0 = 5\lambda$, $\tau = 50$ fs and $\lambda = 1 \mu\text{m}$.

laser propagation direction, and extension 0.6λ in the transverse direction. Here, we assume the electrons (in the hydrogen gas) to be underdense $n_e = 0.1 n_c$, where $n_c = 1.1 \times 10^{21}$ cm⁻³ is the critical density for $\lambda = 1 \mu\text{m}$ wavelength. For the protons, the total number per shot being accelerated as one bunch amounts to $\approx 10^7$.

Fig. 3 provides an insight into the acceleration mechanism and the plasma dynamics. From Fig. 3 (a), we can see that when the laser pulse approaches the gas target, the electrons get blown off the target. The density profile of the electrons follows approximately the laser field oscillation. At this time ($t = 16$ laser cycles) the proton distribution almost maintains its initial shape. After the interaction of the gas target with the laser pulse, we see from Fig. 3 (b) that the protons are accelerated as a symmetric bunch of homogeneous density (average density at $t = 50$ laser cycles: $\bar{n}_p \approx 0.04 n_c$). Note that the proton bunch is emitted at 70° relative to the laser propagation direction (z -direction). Due to the comparatively low density of the plasma target and, hence, suppressed Coulomb explosion, the time-dependent beam divergence is low. For a macroscopic distance of 30 cm, the cross-

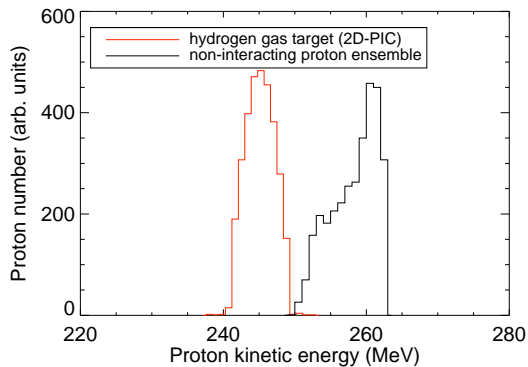


FIG. 4: (color online). Proton kinetic energy distributions after the interaction of a chirped laser pulse ($b = -0.003033$) with a hydrogen gas target (left peak) and with an ensemble of protons without particle-particle interaction effects (right peak). The laser peak intensity is 2.55×10^{21} W/cm² for both cases.

sectional area of the beam is about 0.98 cm². This number roughly corresponds to a divergence angle (opening angle of the cone defined by the beam) of only 2°. From the particle dynamics it is obvious that the prevailing part of the proton's kinetic energy is transferred via direct interaction with the laser field.

In Fig. 4 we compare the exit kinetic energy distribution of 3000 initially randomly distributed non-interacting particles (cf. [35, 36] for the method) in a spatial volume with the same dimensions as the gas target (cf. Fig 3 (a)), with the one stemming from the laser – gas target interaction. In the case of pure vacuum acceleration $K = 258.3$ MeV \pm 1.2%, while for the laser-plasma-cell acceleration $K = 245.2$ MeV \pm 0.8%. The discrepancy between the reported mean kinetic energies is about 5%, which can be attributed to particle-particle interaction effects. Moreover, the simulation of the randomly distributed non-interacting particle ensemble has been carried out in three spatial dimensions, whereas the PIC simulation is two dimensional. Enlarging the initial plasma distribution leads to an increase in the energy spread and to a decrease in the mean kinetic energy of the created proton beam. For example a gas target with initial length of 1λ (5 times larger than before) yields $K = 245.1$ MeV \pm 5.4%. However, employing some velocity filter one could maintain the beam quality. In order to reach similar particle energies by using an unchirped laser pulse one would have to raise the laser intensity by three orders of magnitude, to 10^{24} W/cm². At such an intensity the chirped laser scheme (employing the same parameters as in Fig. 2) already yields monoenergetic proton beams with $K = 17.3$ GeV \pm 1.0%.

In summary, we have demonstrated the theoretical feasibility of creating a dense proton beam (10^7 protons per bunch) of high energy (≈ 250 MeV) and good quality (energy spread $\sim 1\%$), from the interaction of a chirped laser

pulse with an underdense hydrogen gas target. The required laser peak intensity of about 10^{21} W/cm² is within the range of state-of-the-art high-intensity laser systems [22]. Furthermore, we developed an analytical model for determining the optimal pulse shape and the final kinetic energy of the particles, which is in good agreement with the performed 2D-PIC simulations. Our work has mainly been concerned with proton acceleration to energies and densities required for hadron therapy. Following acceleration, ion beam shaping [24] beyond the scope of the present Letter has to be applied.

BJG acknowledges discussions with T. Pfeifer. YIS is supported by the Arab Fund for Economic and Social Development (State of Kuwait). Supported by Helmholtz Alliance HA216/EMMI.

-
- [1] B. M. Hegelich *et al.*, Nature **439**, 441 (2006).
 - [2] H. Schworer *et al.*, Nature **439**, 445 (2006).
 - [3] J. Fuchs *et al.*, Nature Physics **2**, 48 (2006).
 - [4] L. Robson *et al.*, Nature Physics **3**, 58 (2007).
 - [5] R. A. Snavely *et al.*, Phys. Rev. Lett. **85**, 2945 (2000).
 - [6] S. Karsch *et al.*, Phys. Rev. Lett. **91**, 015001 (2003).
 - [7] L. Romagnani *et al.*, Phys. Rev. Lett. **95**, 195001 (2005).
 - [8] T. Tajima, J. M. Dawson, Phys. Rev. Lett. **43**, 267 (1979).
 - [9] A. J. Mackinnon *et al.*, Phys. Rev. Lett. **86**, 1769 (2001).
 - [10] A. Maksimchuk, S. Gu, K. Flippo, D. Umstadter, V. Y. Bychenkov, Phys. Rev. Lett. **84**, 4108 (2000).
 - [11] P. Mulser, D. Bauer, and H. Ruhl, Phys. Rev. Lett. **101**, 225002 (2008).
 - [12] T. V. Liseykina, S. Pirner, and D. Bauer, Phys. Rev. Lett. **104**, 095002 (2010).
 - [13] F. Peano *et al.*, IEEE Trans. Plasma Sci. **36**, 1857 (2008).
 - [14] M. Dunne, Science **312**, 374 (2006).
 - [15] S. E. Combs *et al.*, Cancer **115**, 1348 (2009).
 - [16] O. Jäkel, M. Krämer, C. P. Karger, J. Debus, Phys. Med. Biol. **46**, 1101 (2001).
 - [17] G. A. Mourou *et al.*, Rev. Mod. Phys. **78**, 309 (2006).
 - [18] A. Macchi *et al.*, Phys. Rev. Lett. **103**, 085003 (2009).
 - [19] A. Henig *et al.*, Phys. Rev. Lett. **103**, 245003 (2009).
 - [20] S. V. Bulanov *et al.*, Phys. Rev. Lett. **104**, 135003 (2010).
 - [21] H. Eickhoff *et al.*, *HIT-Heidelberg Ion beam Therapy. Scientific Case.*, http://www-aix.gsi.de/~spiller/facilit_ep00.ps.
 - [22] S.-W. Bahk *et al.*, Opt. Lett. **29**, 2837 (2004).
 - [23] J. Weichsel *et al.*, Phys. Med. Biol. **53**, 4383 (2008).
 - [24] M. Schollmeier *et al.*, Phys. Rev. Lett. **101**, 055004 (2008).
 - [25] *The Extreme Light Infrastructure European Project (ELI)*, <http://www.extreme-light-infrastructure.eu/pictures/ELI-scientific-case-id17.pdf>.
 - [26] *High Power Laser Energy Research (HiPER)*, <http://www.hiperlaser.org/docs/tdr/HiPERTDR2.pdf>.
 - [27] E. Goulielmakis *et al.*, Opt. Lett. **33**, 1407 (2008).
 - [28] R. K. Shelton *et al.*, Science **293**, 1286 (2001).
 - [29] H.-S. Chan *et al.*, Science **331**, 1165 (2011).
 - [30] K. P. Singh, Appl. Phys. Lett. **87**, 254102 (2005).
 - [31] F. Sohbatzadeh, S. Mirzanejad, and M. Ghasemi, Phys.

- Plasmas **13**, 123108 (2006).
- [32] F. Sohbatzadeh, S. Mirzanejhad, and H. Aku, Phys. Plasmas **16**, 023106 (2009).
- [33] Y. I. Salamin, Appl. Phys. B **86**, 319 (2007).
- [34] F. Peano *et al.*, Phys. Plasmas **14**, 056704 (2007).
- [35] Y. I. Salamin, Z. Harman, C. H. Keitel, Phys. Rev. Lett. **100**, 155004 (2008).
- [36] B. J. Galow, Z. Harman, C. H. Keitel, Opt. Express **18**, 25950 (2010).